TPM Vol. 32, No. S3, 2025
ISSN: 1972-6325
https://www.tpmap.org/

Open Access

AERODYNAMIC STUDY OF THE SPEEDS AND PRESSURES OF A CROSS-VAULT STYLE GREENHOUSE THROUGH AUTODESK CFD SOFTWARE

DANNA JAMILA VERA ORTEGA[A,*], JUAN ANTONIO BALDEON SOSA[A], ABEL CARMONA ARTEAGA[A], JHON HENRY RODRÍGUEZ POMAJULCA[A]

[A] UNIVERSIDAD PRIVADA DEL NORTE, LIMA, PERÚ.

ABSTACT: In recent years, the impact of wind on structures has become an increasing concern, particularly in areas affected by extreme climatic conditions. This research focuses on the aerodynamic design and analysis of a greenhouse optimized for these conditions, using Autodesk CFD software to evaluate wind distribution and pressure on the structure. The design is based on a mathematical surface described by the equation $z = \mathrm{acos}(\mathrm{Sqrt}(\cos(xy)))$, forming a ribbed vault. Additionally, Autodesk Inventor was used to create a 3D model of the simulated structure. The simulation results reveal variations in wind speed around the surface and the location of negative pressure zones, which helped identify the most vulnerable areas and improve aerodynamic efficiency under adverse climatic conditions. To validate these results, comparative tests were conducted using a wind tunnel and a scaled prototype of the structure. This study demonstrated the effectiveness of aerodynamic simulation software, providing a deeper understanding of wind behavior and its impact on buildings. The findings can contribute to the development of more resilient and efficient structures in areas with extreme climatic conditions, fostering innovative solutions in the design of agricultural infrastructure and buildings.

Keywords: Aerodynamics Autodesk CFD Greenhouse Mathematical Surfaces Ribbed Vault Wind Tunnel

INTRODUCTION

In recent years, many structures have collapsed due to the forces exerted by the wind, primarily as a result of underestimating this load [1]. Changes in wind speed and their impact on structures have been topics of significant interest and concern in the construction industry. Wind can generate substantial forces on buildings, causing stresses and deformations that, if not properly managed, can lead to structural failure.

As time progressed, innovations emerged to implement buildings that met this purpose. As construction techniques advanced, the need arose for more efficient structures that could be modified according to architectural requirements.

This is the case for surfaces designed based on mathematical equations, which often aim to emulate existing designs while increasing their complexity to adapt to new environments where they are needed. These surfaces are created using mathematical algorithms that define their shape and structure. Similarly, they offer greater flexibility and precision in architectural design, as they can be adjusted and optimized to meet specific load and resistance requirements.

The use of these equations gives rise to curvilinear and complex forms that can minimize stress points and reduce areas of high pressure, resulting in more stable and durable constructions. Among these forms are double-curvature surfaces, which are common in structures such as ribbed vaults. These structures benefit from their own weight to achieve stability. As the size increases, self-weight surpasses additional loads, preventing collapse and allowing for more slender and efficient designs [2].

Ribbed vaults, with their interlocking ribs, are particularly well-suited for structures that require both strength and lightness. This design efficiently distributes weight, allowing for greater heights and spans without compromising stability. These characteristics are essential in greenhouse architecture, where the need to create a controlled environment for plant cultivation coincides with the requirement to withstand adverse climatic conditions. Due to their lightweight, low stiffness, and high flexibility, ribbed vaults are highly sensitive to wind loads. Therefore, these loads are critical in the design of greenhouses to ensure structural reliability [3].

As previously emphasized, in addition to structural strength, aerodynamics is a crucial factor that must be considered. An efficient design can minimize wind resistance and distribute pressures evenly, thereby reducing the risk of damage and enhancing the stability of the construction. Although arch structures are very popular today, there is still a need for comprehensive research to more accurately estimate wind loads and define the characteristics of wind pressure distribution [1].

Based on this premise and highlighting the limited information available related to this specific topic, it is possible to obtain insights with the aid of technology. A viable solution for this issue is the use of Autodesk CFD, which is effective for performing simulations as well as analyzing and visualizing the aerodynamic environment in greenhouses [4].

This tool allows us to study airflow behavior and pressure conditions in various designs. Utilizing the information provided earlier, the following question arises: How can we understand the behavior of velocities and pressures on a ribbed vault greenhouse model, and how does this design affect aerodynamic performance? This research aims to analyze the distribution of velocities and pressures on a greenhouse design based on the mathematical surface model z=acos(Sqrt(cos(xy))), which simulates the design of a ribbed vault. This will be conducted both experimentally, using a wind tunnel, and computationally, using Autodesk CFD, to evaluate the locations where drag forces will act on the structure.

1.1 Energy Equation

The general energy equation, known as an extension of Bernoulli's equation, allows for the analysis of fluid behavior through a flow system by considering two sections of the system [5]. The general energy equation can be seen in Equation (1).

$$\frac{p_1}{\gamma}+z_1+\frac{v_1^2}{2g}=\frac{p_2}{\gamma}+z_2+\frac{v_2^2}{2g}+h_t \qquad (1)$$

p_1= Gauge pressure in the first section.
γ = Specific weight of the fluid.
z_1 = Position height in the first section.
v_1 = Fluid velocity in the first section.
g = Gravity.
p_2 = Gauge pressure in the second section.
V_2 = Fluid velocity in the second section.
z_2 = Position height in the second section.
h_T = Total losses due to friction and accessories.

1.2 Von Kármán Effect

The effect of vortex shedding, also known as the "Vortex Street effect," was first described and mathematically formalized by Theodore von Karman, the genius of aeronautics, in 1911. This effect is produced by the lateral forces of the wind on an object immersed in laminar flow. The wind flow generates a cyclical pattern of vortices, which can pose an engineering challenge for slender structures such as towers, masts, and chimneys [6].

1.3 Drag Force

n a particle system, when bodies are submerged in a moving fluid, they are subjected to a force with two components known as drag force. The two components are the friction exerted by the fluid and the form drag, which depends on the pressure distribution acting on the object [7]. The equation for drag force is presented in Equation (2).

$$F_D=C_D\times A\times\frac{v^2\times\rho}{2} \qquad (2)$$

F_D = Drag force.
C_D = Drag coefficient.
A = Front area.
V = Fluid velocity.
$\boldsymbol{\rho}$ = Density of the fluid.

1.4 Navier-Stokes Equation

The Navier-Stokes equation allows us to determine the motion of a fluid at any given moment, whether it is ideal or viscous [8]. The reduced form of the Navier-Stokes equation is presented in Equation (3).

$$\rho\left(\frac{\partial v}{\partial t}+\left(v\cdot\Delta\right)v\right)=-\Delta p+\rho g+\eta\nabla^2 v \qquad (3)$$

ρ = Fluid density.
v = Fluid velocity.
t = Time.
p = Fluid pressure.
η = Absolute viscosity coefficient.
g = Gravity.

1.5 Lift Force

The lift force is the perpendicular component of the force exerted by an airflow on a body, resulting from pressure fields and shear stresses on its surface [9]. The lift force is presented in Equation (4).

$$F_L = C_L \times A \times \frac{V^2 \times \rho}{2} \quad (4)$$

F_L = Lift force.
C_L = Lift coefficient.
A = Front area.
V = Fluid velocity.
ρ = Fluid density

1.6 Reynolds Number

The Reynolds number is a dimensionless value that compares inertial forces to viscous forces in a fluid. This number determines the transition of fluid flow [10]. When the Reynolds number is below 2300, the flow is considered laminar; however, if it exceeds 2300, the flow is deemed turbulent. The Reynolds number is presented in Equation (5).

$$\mathrm{Re} = \frac{D_h \cdot v \cdot \rho}{\mu} \quad (5)$$

D_h = Hydraulic diameter.
V = Fluid velocity.
ρ = Fluid velocity.
μ = Fluid viscosity.

1.7 Turbulence in CFD

Turbulence is a dynamic and chaotic phenomenon that occurs in most flows with high Reynolds numbers. It is characterized by rapid and irregular variations in fluid properties, such as pressure and velocity. Accurately representing and predicting these motions remains one of the major challenges in computational fluid dynamics (CFD). To address this, AUTODESK CFD provides various simulation methods that differ in terms of accuracy and computational demand. [11].

1.8 Selection of the Model Based on Flow Physics

Laminar flows or flows with a low Reynolds number: When the flow is orderly and characterized by a low Reynolds number, a turbulence model is not required.

Steady turbulent flows (RANS models): In most practical cases where a balance between accuracy and computational efficiency is required, Reynolds-Averaged Navier-Stokes (RANS) models, such as k-epsilon and k-omega SST, are employed. These models are well-suited for applications involving duct flows, ventilation, structural aerodynamics, and fluid transport system design.

Transient flows and large turbulent structures (LES models): When capturing large-scale turbulent structures that evolve over time is crucial, Large Eddy Simulation (LES) models, such as Smagorinsky or Dynamic Smagorinsky, are more appropriate. These models are employed in simulations of flows around complex geometries, vehicle aerodynamics, vortex formation prediction, and atmospheric flow simulations.

High-precision complex flows (DNS): When it is necessary to resolve all turbulence scales without approximation models, Direct Numerical Simulation (DNS) is employed. Although it offers extremely high accuracy, its significant computational cost restricts its application to academic research, model validation, and fundamental fluid dynamics studies, particularly in flows with low Reynolds numbers.

1.9 Recommendations for Selecting a Turbulence Model

Start with simplified models: If there is limited experience in turbulence simulation, it is advisable to begin with RANS models, such as k-epsilon or k-omega SST, as they provide a balance between accuracy and efficiency without demanding excessive computational resources.

Consider computational demand: If resources are limited, RANS models are the most suitable option, as they require less processing time and computational power. However, if capturing more complex turbulent structures is necessary, LES can be considered, although it entails significantly higher computational requirements.

Application in designs with complex geometries: When working with geometries that involve boundary layer separation or intricate structures, it is preferable to use LES or more advanced RANS models, such as k-omega SST, as they provide more accurate results in these scenarios.

Flows near solid surfaces: For flows in proximity to solid surfaces, such as in aerodynamics or wind-exposed structures, k-omega SST or WALE (LES) models are suitable, as they enable a more accurate representation of flow-surface interactions.

1.10 Law of Similarity

The law of dynamic similarity is a principle used in fluid engineering and aerodynamics to ensure that the results from a scale model are representative of the behavior of a real prototype. This law implies that models and prototypes must have similar geometric proportions and flow relationships [12].

1.11 Ribbed Vault

The ribbed vault is a versatile architectural system that represented a significant improvement over other methods, as it facilitated both the design and construction process, as well as the adaptation to various ground plan geometries. This structure is composed of two main elements: the ribs and the webbing. The ribs act as guides during construction, forming a framework over which the webbing, a double-curved surface that closes the space, is placed. This method allows for an efficient definition of the vault through the arrangement of linear arches [13].

1.12 Autodesk Fusion

Autodesk Fusion 360 is computer-aided design (CAD) software that enables rapid design exploration through AGD technology. This software generates multiple solutions simultaneously based on manufacturing constraints, costs, and product performance requirements. The generated solutions are compatible with any CAD/CAM system [14].

1.13 Autodesk Inventor Professional

Autodesk Inventor is CAD software for creating 3D models by combining solids and surfaces. It uses three-dimensional basic bodies and algorithms to form complex geometries by combining, cutting holes, and sweeping cross-sections. It is essential for engineers and designers in product visualization and simulation [15].

1.14 Autodesk CFD

The Autodesk CFD program integrates disciplines such as fluid dynamics, computational methods, and computer graphics. CFD numerical simulation involves solving the fundamental equations that govern the movement of fluids using numerical methods to simulate the behavior of fluids. This allows for the derivation of discrete physical quantities in the field, such as win speed and direction, at different spatial locations [16].

1.15 Wind Tunnel

A wind tunnel is a research tool used to simulate and study airflow behavior around objects or scale models, replicating specific atmospheric conditions. It allows for the observation and measurement of parameters such as wind speed, turbulence intensity, and wind profile relative to height. Wind tunnel tests aim to meet similar criteria between the model and the real prototype to obtain representative results [17].

Scale models are generally used to reduce costs or because the actual object is too large. However, the size of the model affects the test results, the larger and more realistic the model, the better the experimental outcomes. Various elements and variables such as pressures, forces, boundary layer information, and flow streamlines can be visualized and measured, depending on the object being tested and the desired results [18].

METHODOLOGY

To carry out this research, measurements were first taken from the wind tunnel of the Universidad Privada del Norte at the Breña campus, with these measurements we carried out the 3D modeling of the wind tunnel using the Inventor program. Then, the model to be studied was established using a mathematical equation that could form a surface like the structure of a ribbed vault. Equation (6) shows the study model.

$$f(x,y) = a\cos\left(sqtr\left(\cos(xy)\right)\right) \qquad (6)$$

Equation (6) was loaded into an online 3D graphed called CalcPlot3D. This tool allows us to determine the meshing and thickness of the surface, as well as download the information in format .STL. This process can be seen in Fig. 1.

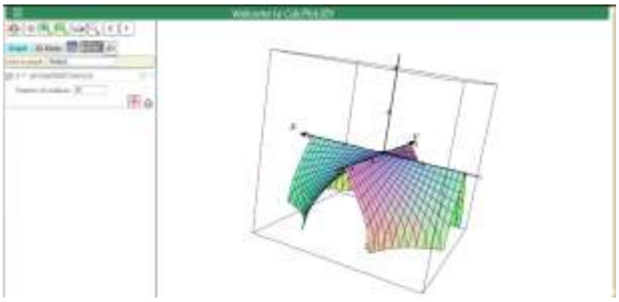

Fig. 1. Three-dimensional surface model using CalcPlot3D [19].

Using Autodesk Fusion 360, as shown in Fig. 2, the file in format .STL was converted to a .STEP, which can be read by Autodesk Inventor. After this, the file in format .STEP was loaded into Autodesk Inventor to scale and modify the hollow parts of the solid. Subsequently, the file was saved in format .IPT.

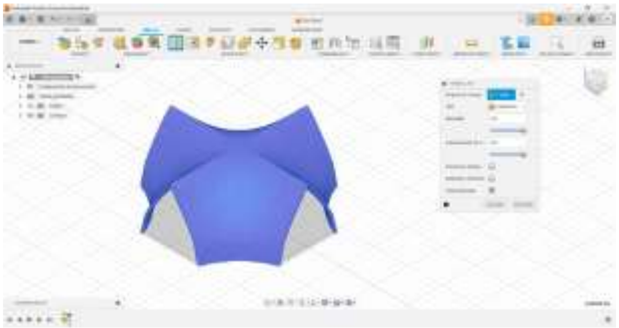

Fig. 2. Creation of the three-dimensional solid using Autodesk fusion 360.

The transformed file, now with the extension .IPT, along with the simulated wind tunnel, were uploaded in format .IAM, which was used within the Autodesk CFD software.

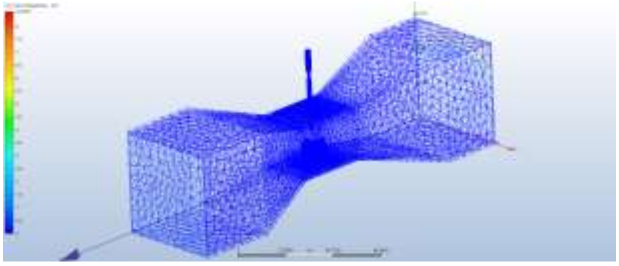

Fig. 3. Creation of the mesh in the wind tunnel.

Within the Autodesk CFD program, the simulation was carried out, in which it was necessary to create a meshing of the tunnel with the object inside it, as shown in Fig. 3. This mesh was generated to solve the Navier-Stokes equations by points using finite difference numerical methods, allowing a more accurate simulation of the behavior of the airflow inside the wind tunnel. In the diagram of Fig. 4, the construction process diagram used for this research work can be seen.

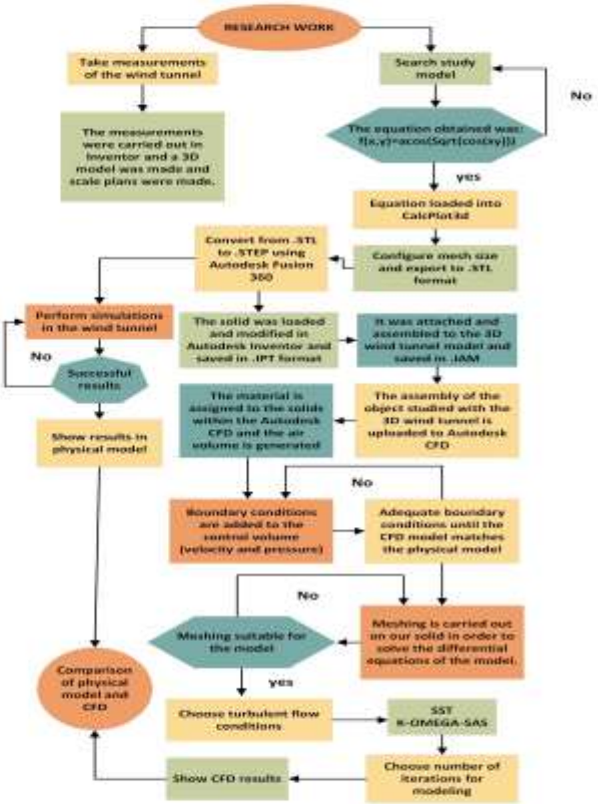

Fig. 4. Work flowchart for the research process.

RESULTS

This section analyses and compares the results obtained both computationally and experimentally for the physical and virtual models of a mathematical surface resembling a ribbed vault. For the CFD simulation, the following conditions were established: the flow was considered incompressible and steady, and only pressure and velocity variables were considered.

Two different cases were analysed, each corresponding to a distinct flow of velocity. This allowed us to obtain more precise and comparable results to assess the aerodynamics of the model. The object was placed in the wind tunnel under identical conditions for both simulations, with the goal of verifying that our model meets the necessary conditions to be classified as aerodynamic.

3.1. Simulation Results with Autodesk CFD

The values of the velocities used in the simulation with Autodesk CFD were 1 m/s and 5 m/s. The gauge pressure at the entrance of the wind tunnel was 30 Pa for both cases. To perform the simulation, it was assigned about 4000 iterations, but the program found a solution in 522 iterations for the first speed and in 608 iterations for the second case. The following figures show the velocity and pressure fields obtained from the simulations, observing the flow in three different views.

A. Simulation Results with Autodesk CFD

The results obtained with the inlet velocity 1m/s, inlet pressure 30 Pa and outlet pressure 0 Pa in a side view are shown in Fig. 5. It is observed that the velocity of entry of the fluid through the wind tunnel is 1 m/s, but when it reaches approximately the lower half of the object, it generates the stagnation point and then disperses in all directions. When it reaches the top of the object, the velocity of the flow rises to an interval of 3.20 to 5.88 m/s, close to the area where the velocity reaches its highest point, in addition to the posterior area of the solid a trail is formed in which the velocities begin to decrease reaching a minimum value of 0 m/s.

Fig. 6 shows in more detail the formation of the wake at the back of the solid and the stagnation point in the frontal area, where the velocity is very low, with an interval of 0 to 1.60 m/s. On the sides, the flow area is reduced and the velocity increases, reaching values between 4.81 and 7.48 m/s. In this area are located the points of detachment, where the flow moves away and takes another direction.

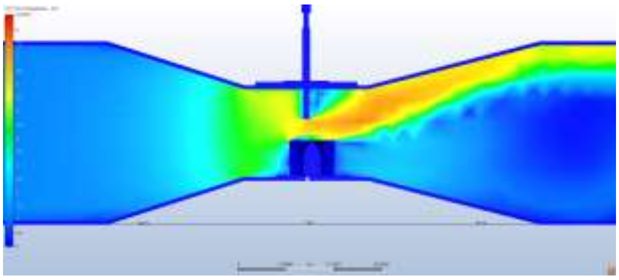

Fig. 5. Side view of the velocity distribution for flow inlet conditions at 1m/s.

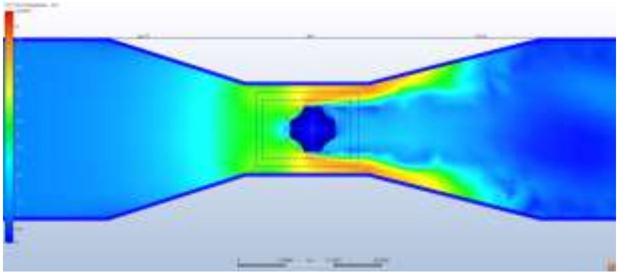

Fig. 6. Plan view of the velocity distribution for flow inlet conditions at 1m/s.

In the case of the front view, in Fig. 7, it is possible to visualize how the flow advanced through the solid. The velocity begins to increase in magnitude as it separates from the solid, registering a velocity with values between 6 to 7.5 m/s.

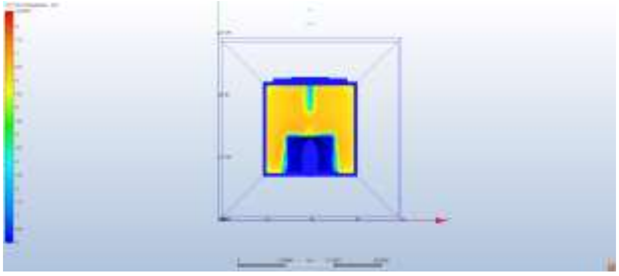

Fig. 7. Front view of the velocity distribution for flow inlet conditions at 1m/s.

In view of Fig. 8, we can see that the vectors show an acceleration in the narrowing zone and a deceleration at the back of the solid, with a clear recirculation behind the constriction, where the vectors change direction and form circular patterns. These visualizations indicate how the flow accelerates and decelerates, generating drag forces.

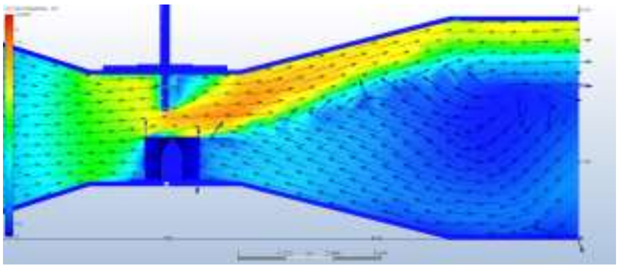

Fig. 8. View of the trajectory of the vectors for the speed of 1m/s.

B. Computational Simulation with a Speed of 5 m/s

Fig. 9 shows the results obtained with an inlet velocity of 5 m/s, an inlet pressure of 30 Pa and an outlet pressure of 0 Pa. The velocities begin to vary as the flow approaches the solid, in the front part where the stagnation point is located, the velocity is very low, reaching the value of 0 m/s, in the same way it happens in the back where the wake is formed. In the upper part, the point of detachment begins to be noticed and as the flow separates from the model, the speed increases, thus reaching a maximum value of 12.79 m/s and then decaying in magnitude until the outlet.

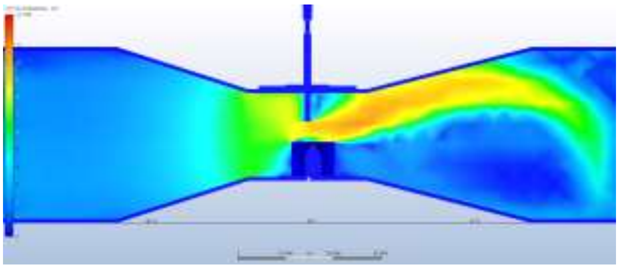

Fig. 9. Side view of the velocity distribution for flow inlet conditions at 5m/s.

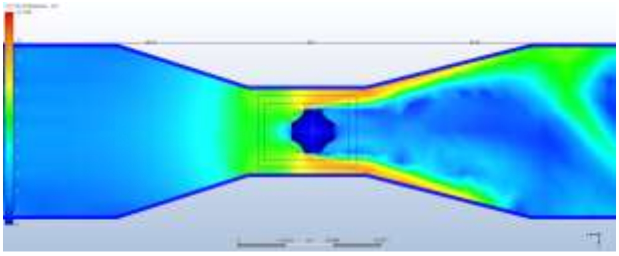

Fig. 10. Plan view of the velocity distribution for flow inlet conditions at 5m/s.

In Fig. 10, it is observed how, at the rear, the wake formed takes a different shape than when a velocity of 1 m/s was assigned. The separation points are located on the sides, and it is notably seen how the velocity increases as the flow area decreases and the flow moves away from the solid. At the front, velocity values are high, but at the stagnation point, it begins to decrease as the flow starts to move along the sides.

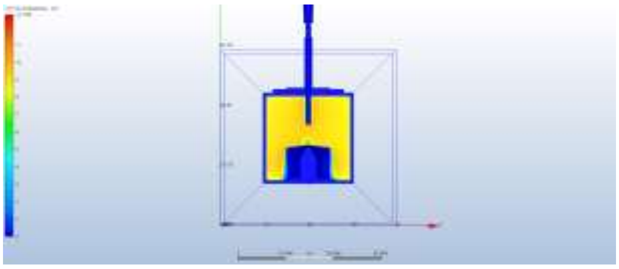

Fig. 11. Front view of the velocity distribution for flow inlet conditions at 5m/s.

Fig. 11 shows that the velocities closest to the solid are higher than those farther away. When close to the solid, they register between 8.74 and 9.54 m/s, indicating how the flow detaches from the figure, reducing the flow's magnitude as it moves away.

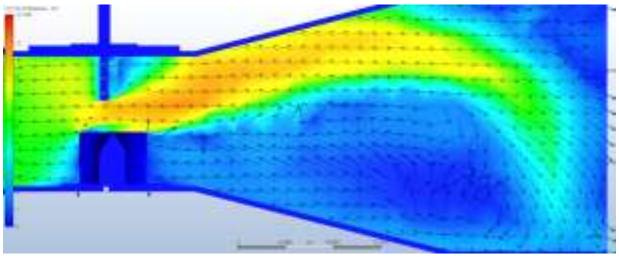

Fig. 12. View of the trajectory of the vectors for the speed of 5m/s.

Fig. 12 shows that the vectors indicate acceleration in the narrow area and a decrease in velocity at the rear and lower rear part of the solid. An evident recirculation is also observed behind the narrowing zone, where the vectors change direction and form circular patterns. These visualizations illustrate how the flow accelerates and decelerates, generating drag forces.

C. Computational Simulation with a Pressure of 30 Pa and Speed of 1 m/s

Fig. 13 shows the pressure distribution. At the front, the pressure reaches high values, up to 30 Pa, while the flow reaches the upper part and begins to separate from the solid, with values starting to decrease at an approximate velocity of 6.28 m/s. In the rear zone, where the wake was formed, there was a significant pressure drop, reaching negative values around -33.26 Pa. As previously observed, the flow reached its maximum velocity in this narrow region.

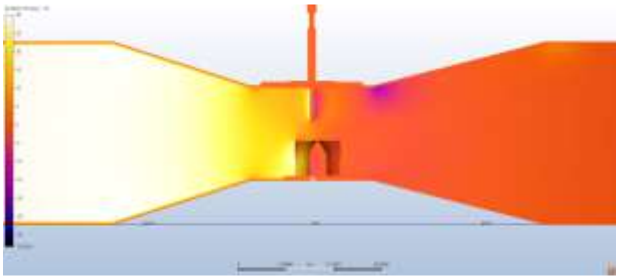

Fig. 13. Lateral view of the pressure distribution for flow inlet conditions at 1m/s.

In Fig. 14, the losses throughout the system can be observed. As the flow moves away from the separation points, shifting to the sides, the pressure noticeably decreases. In this view, the pressure drop in the narrow region of the duct is significant, with negative values of -1.63 Pa, indicating a considerable acceleration of the flow until the end of the narrowing zone, where the pressure decreases to a value of -33.26 Pa.

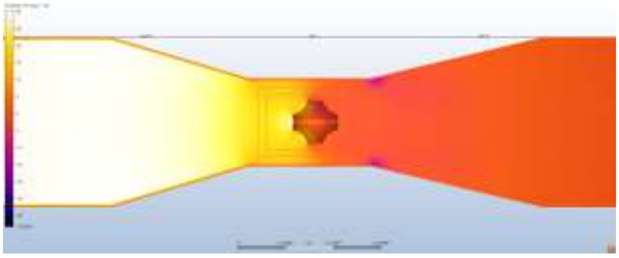

Fig. 14. Plan view of the pressure distribution for flow inlet conditions at 1m/s.

In Fig. 15, we have a frontal view, where the area closest to the model, on the sides, exhibits lower pressures, reaching a value of -13.49 Pa. Conversely, as the flow moves away, the pressures are slightly higher, with values of 10.23 Pa.

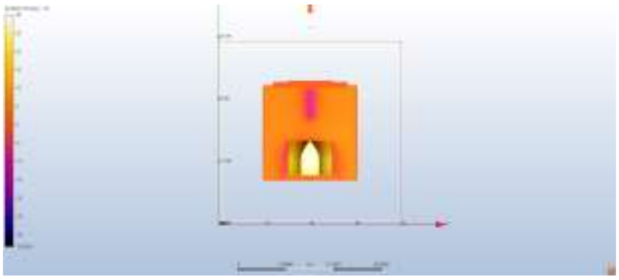

Fig. 15. Front view of the pressure distribution for flow inlet conditions at 1m/s.

D. Computational Simulation with a Pressure of 30 Pa and Speed of 5 m/s

The lateral view of the simulation, shown in Fig. 16, illustrates a slight decrease in pressure as the flow approaches the constriction, reaching values close to 19.79 Pa where the reduced area of the duct causes an increase in flow velocity and a corresponding drop in pressure. In this case, lower pressures were obtained, with the minimum recorded pressure reaching -77.98 Pa, compared to the first case, as the velocity is higher.

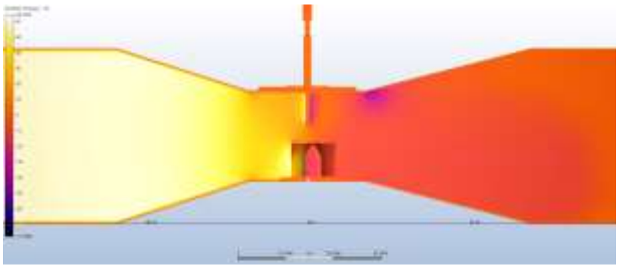

Fig. 16. Lateral view of the pressure distribution for flow inlet conditions at 5m/s.

In Fig. 17, it can be observed that on the sides of the solid, where the separation points are located, regions of negative pressure down to -24.65 Pa are identified, indicating the formation of vortices or recirculating flow zones. This highlights the area where the flow begins to detach.

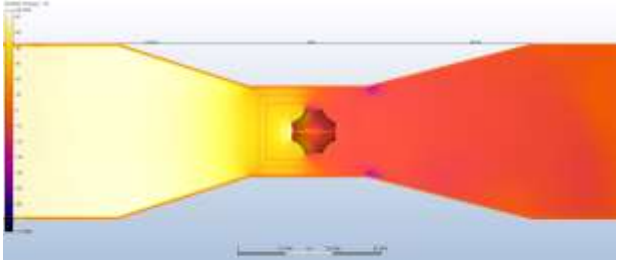

Fig. 17. Plan view of the pressure distribution for flow inlet conditions at 5m/s.

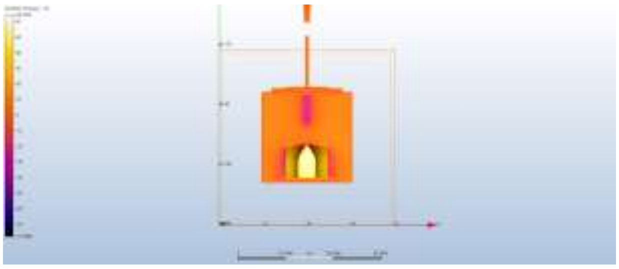

Fig. 18. Front view of the pressure distribution for flow inlet conditions at 5m/s.

The zones with negative pressures on the sides of the model, as shown in Fig. 18, are lower in the areas closest to the solid, particularly on the sides and slightly on the top, with values ranging from -33.54 Pa to -10.90 Pa. In these areas, it can be observed, as in previous images, that as the velocity increases, the pressure decreases.

3.2. Wind Tunnel Simulation Results

Fig. 19 shows the results obtained when the 3D model was simulated inside the wind tunnel, assigning it a speed of 1 m/s. In this experiment, smooth flow lines were generated that closely follow the surface of the model design. These flow lines show how the air moves evenly around the object. However, as it passes over the top of the model, these flow lines deviate and begin to form a wake at the back, where the airflow becomes uneven and becomes turbulent.

Fig. 19. Profile view of the wind tunnel with a flow speed of 1m/s.

Fig. 20. Profile view of the wind tunnel with a flow velocity of 5m/s.

A second simulation was conducted at a velocity of 5 m/s, as shown in Fig. 20. The resulting flow lines are sharper, indicating that as they deviate while passing over the top of the model, the wake formed is slightly larger than in the previous case.

CONCLUSION

During simulations using Autodesk CFD, it was observed that, in the central region of the wind tunnel, where the flow area decreases, the velocity increases significantly, and the pressure drops to negative values. This phenomenon is due to the increase in velocity and the constant change in direction vectors, which intensify frictional losses and generate drag forces. To compensate for the resulting energy loss, the pressure decreases. This relationship can be explained using the general energy equation, which shows how pressure must decrease to balance the increase in velocity and energy losses. Additionally, the von Kármán effect was observed, with the formation of vortices on the lateral sides of the object, which detach and form a wake behind the model.

In the wind tunnel, the flow around the structure was observed and compared to the CFD simulation. The use of smoke allowed for the visualization of the flow, identifying fluid separation and wake formation, with results that were similar to those from the simulation. This confirms the compliance with the laws of dynamic and geometric similarity, as the flow lines and the scales of the model and prototype are very similar. In both cases, the point of separation and the size of the wake were practically identical. After conducting both computational and physical simulations, it was concluded that CFD simulations are useful for analyzing velocity and pressure at each point in the flow. However, due to the multiple external and internal factors within the fluid itself, results may vary. If one were to attempt to account for all these factors in the simulation software, it is likely that a solution would not be achievable.

REFERENCES

[1] X. Sun, A. Kandel y Y. Wu, «Investigation on wind tunnel experiment of oval-shaped arch-supported membrane structures,» Journal of Wind Engineering and Industrial Aerodynamics, vol. 206, nº 104371, 2020. https://doi.org/10.1016/j.jweia.2020.104371

[2] G. Abad Vegas, "El lenguaje secreto del pasado: arcos y bóvedas," Tesis Final de Grado, UPC, Escola Tècnica Superior d'Arquitectura de Barcelona, 2021. http://hdl.handle.net/2117/353789

[3] C. Wang, B. Nan, T. W. Wang, Y. Bai y Y. L. Li, «Wind pressure acting on greenhouses: A review, » International Journal of Agricultural and Biological Engineering, vol. 14, nº 2, 2021. https://www.ijabe.org/index.php/ijabe/article/view/5261

[4] R.-w. K. Kim, J.-g. K. Kim, I.-b. Lee, . U.-h. Yeo , S.-y. Lee y C. Decano-Valentin, «Development of three-dimensional visualisation technology of the aerodynamic environment in a greenhouse using CFD and VR technology, part 1: Development of VR a database using CFD,» Biosystems Engineering, vol. 207, pp. 33-58, 2021. https://doi.org/10.1016/j.biosystemseng.2021.02.017

[5] L. Álvarez Vitola, R. Briceño Miranda, "Diseño y elaboración de un sistema de tuberías para el análisis de la ecuación general de la energía," Trabajo Final de Grado, Universidad de la Costa, 2021. https://hdl.handle.net/11323/8945

[6] D. S. Umaña, «Investigación experimental del máximo aprovechamiento de las características de un fluido libre para generación de energía por medio de vibración inducida por vórtices» Fundación Universitaria Los Libertadores, 2020. http://hdl.handle.net/11371/3171

[7] A. Meza de Luna, A. Nolasco López, . A. I. García Castañón, F. Chávez Valdivia, R. B. Sierra Ortiz y R. Reyes Cortes, «Simulación Aerodinámica de Propuesta de Motocarro Eléctrico Mexicano Mediante Coeficiente de Arrastre y Sustentación,» Pistas Educativas, vol. 44, nº 143, 2022. https://pistaseducativas.celaya.tecnm.mx/index.php/pistas/article/view/2831

[8] F. J. Zamora Picón, "Soluciones a la Ecuación de Navier-Stokes," Grado en Matemáticas, Universidad de Almería, Almería, España, 2021. http://hdl.handle.net/10835/13165

[9] N. Sautié, L. Romero Monteiro, E. B. Camano Schettini y V. E. Parnás, «Determinación de los coeficientes de arrastre y sustentación en un perfil angular de alas iguales con el empleo de simulación numérica,» Ingeniería y Desarrollo, vol. 38, nº 1, 2021. http://www.scielo.org.co/scielo.php?pid=S0122-34612020000100066&script=sci_arttext

[10] M. Duran, J. A. Villabona, y B. E. T. Romero, «Evaluación de la pérdida de energía en un fluido en tuberías de diferente material, usando la ecuación de Darcy-Weisbach, mediante la variación de temperatura y caudal», ResearchGate, nov. 2021. https://www.researchgate.net/publication/356616585_Evaluacion_de_la_perdida_de_energia_en_un_fluido_en_tuberias_de_diferente_material_usando_la_ecuacion_de_Darcy-Weisbach_mediante_la_variacion_de_temperatura_y_caudal

[11] R. I. Ponce Segovia, *Dinámica de Fluidos computacional con OpenFOAM: Fundamentos y estrategias avanzadas*. 1nd. ed. Columbia, USA: CFD.PERU-CFD.NINJA-NSIV.IO, 2004.

[12] E. Hernández, D. López, and P. González, «Liderazgo y calidad en los centros educativos: una revisión sistemática de la literatura», Redalyc, vol. 10, no. 4, pp. 1-19, Mar. 2023. https://produccioncientificaluz.org/index.php/tecnica/article/view/27421

[13] A. González, «Estudio de caso sobre el impacto del cambio climático en la agricultura en Aragón», Universidad de Zaragoza, 2023. https://doi.org/10.4995/ega.2023.19387

[14] M. Singh, P. R. Thakur, and A. S. Rani, «A novel framework for the optimization of energy consumption in IoT-based smart homes», Procedia Computer Science, vol. 240, no. 589, pp. 6638-6645, 2023. https://doi.org/10.1016/j.ifacol.2023.10.307

[15] L. Smith and R. Johnson, «Application of machine learning techniques in predictive maintenance», Applied Sciences, vol. 10, no. 15, pp. 5033-5045, 2020. https://doi.org/10.3390/app10155033

[16] F. Qian, Z. Shi, and L. Yang, «Thinking of Green, Low Carbon, and Energy-Saving Designs Based on the Variable Ventilation of Natatoriums: Taking the Jiading Natatorium of Tongji University as an Example», Sustainability, vol. 16, no. 4476, pp. 1-20, Jun. 2024. https://doi.org/10.3390/su16114476

[17] Y. Zhao, R. Li, L. Feng, Y. Wu, J. Niu y N. Gao, «Boundary layer wind tunnel tests of outdoor airflow field around urban buildings: A review of methods and status», Renewable and Sustainable Energy Reviews, vol. 2022, no. 6062, pp. 1-15, Jun. 2022. https://doi.org/10.1016/j.rser.2022.112717

[18] N. Balduzzi y N. Balduzzi, «Diseño y construcción de un túnel de viento supersónico con sistema de visualización Schlieren», Tesís de titulación, Facultad de Ingeniería, Universidad Nacional de la Plata, La Plata, Argentina, 2022. https://doi.org/10.1016/j.rser.2022.112717

[19] CalcPlot 3D, Ecuación z=acos(Sqrt(cos(xy))). https://c3d.libretexts.org/CalcPlot3D/index.html